



This is a repository copy of *A general modelling technique for a triple redundant 3x3-phase PMA SynRM*.

White Rose Research Online URL for this paper:
<http://eprints.whiterose.ac.uk/126262/>

Version: Accepted Version

Article:

Wang, B., Wang, J., Griffo, A. orcid.org/0000-0001-5642-2921 et al. (1 more author) (2018) A general modelling technique for a triple redundant 3x3-phase PMA SynRM. IEEE Transactions on Industrial Electronics, 65 (11). pp. 9068-9078. ISSN 0278-0046

<https://doi.org/10.1109/TIE.2018.2793229>

© 2018 IEEE. Personal use of this material is permitted. Permission from IEEE must be obtained for all other users, including reprinting/ republishing this material for advertising or promotional purposes, creating new collective works for resale or redistribution to servers or lists, or reuse of any copyrighted components of this work in other works. Reproduced in accordance with the publisher's self-archiving policy.

Reuse

Items deposited in White Rose Research Online are protected by copyright, with all rights reserved unless indicated otherwise. They may be downloaded and/or printed for private study, or other acts as permitted by national copyright laws. The publisher or other rights holders may allow further reproduction and re-use of the full text version. This is indicated by the licence information on the White Rose Research Online record for the item.

Takedown

If you consider content in White Rose Research Online to be in breach of UK law, please notify us by emailing eprints@whiterose.ac.uk including the URL of the record and the reason for the withdrawal request.



eprints@whiterose.ac.uk
<https://eprints.whiterose.ac.uk/>

A General Modelling Technique for a Triple Redundant 3x3-phase PMA SynRM

Bo Wang, *Member IEEE*, Jiabin Wang, *Senior Member, IEEE*, Antonio Griffo, *Member IEEE*, Bhaskar Sen, *Member IEEE*

Abstract—A general modelling technique is proposed for a triple redundant 3x3-phase permanent magnet assisted synchronous reluctance machine (PMA SynRM). The magneto-motive force (MMF) of the machine is divided into three parts each associated with one 3-phase set. The MMF of each 3-phase set can be described by four variables: d - and q -axis components of the currents, the rotor angle and an MMF offset component which captures the mutual coupling between three 3-phase sets. Therefore the complete machine behavior in all operating conditions can be captured by means of 4-dimensional (4D) tables, which store the flux linkage and torque information. The 4D tables are produced by finite element (FE) analysis for one 3-phase set. As a result, the machine behavior can be predicted by interpolating the 4D tables. The model is capable of representing healthy and fault operations, including unequal current operation in three 3-phase sets, and offers great flexibility for performance assessment, post fault control and fault detection. Its effectiveness is verified by extensive FE simulation and experimental tests in different operation modes.

Index Terms—Fault tolerant, fault modelling, permanent magnet assisted synchronous reluctance machine, multi-phase machine, magneto-motive force, MMF reconstruction.

I. INTRODUCTION

FAULT tolerant machines are being favored in safety critical applications where uninterrupted operation during fault conditions are required. Fault tolerant drives have been reported in the electric traction [1] and aerospace actuation [2], not only providing high reliability and high efficiency powertrains, but also improving the system flexibility and functionality.

For the fault tolerant machine-drive system, the fault behavior should be carefully assessed to ensure it can cope with the fault. The maximum available torque capability should be identified after the fault [3]. New voltage harmonics would appear which pose an extra demand on the voltage if field weakening is required [4]. In addition, in order to

optimize the output capability in fault condition, accurate fault modelling is necessary to guide machine design and control strategies leading to higher efficiency and power density [5]. Fault modelling also facilitates the development of diagnostic techniques [6]. Thus, the fault modelling of the drive system is worth investigation.

Parameter based modelling is commonly employed to describe the machine in both healthy and fault conditions. The inductance values may be extracted from numerical derivations [7], FE simulations [8] or experimental tests [9]. Circuit-oriented method is an alternative way to investigate the induction machine [10] which can model the faults in both stator and rotor sides, such as inter-turn short circuit or broken rotor bar. A five phase synchronous reluctance machine with open circuit faults was modelled in the synchronous frame in [11]. Other approaches use the winding function to calculate inductances which are derived by integrating the product of turn function, winding function and airgap permeance [12, 13]. A novel field reconstruction method was used to analyze the machine performance and vibration [14]. This method utilized the fields created by the current in a single slot and the fields induced by the magnets to reconstruct the field distribution along the airgap with arbitrary current excitation. It should be noted that most of the modelling methods above consider the machine as a linear system, and hence compromise the model accuracy.

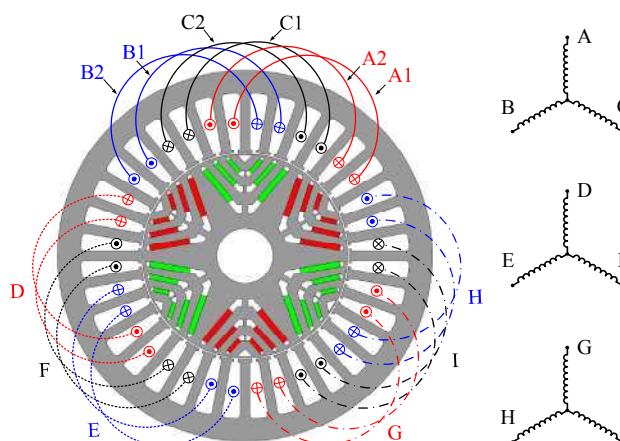


Fig. 1. Triple redundant PMA SynRM with segregated windings.

A triple redundant 3x3-phase PMA SynRM whose cross-section is shown in Fig. 1, was initially proposed in [15]. The conventional overlapped windings are divided into three sets of separated 3-phase windings with each set non-overlapped,

Manuscript received August 24, 2017; revised November 04, 2017; accepted December 28, 2017.

Copyright (c) 2014 IEEE. Personal use of this material is permitted. However, permission to use this material for any other purposes must be obtained from the IEEE by sending a request to pubs-permissions@ieee.org.

The authors are with the Department of Electronic and Electrical engineering, The University of Sheffield, Sheffield, S1 3JD United Kingdom (e-mail: bowang.ee@hotmail.com; j.b.wang@sheffield.ac.uk; a.griffo@sheffield.ac.uk; bsen.ee@gmail.com).

resulting in physical and thermal isolation. Each 3-phase set is star-connected and driven by an independent standard 3-phase inverter. The three neutrals are not connected together to ensure electrical isolation. In case of an open circuit fault, the fault set is deactivated by opening all the switches. If a short circuit failure occurs in the switches or windings, a terminal short circuit can be applied to the faulty set by closing all the bottom or the top switches of the respective inverter. Thus, owing to the winding separation, other parts of the machine are isolated and can continue operation. As a result, the PMA SynRM with segregated winding configuration exhibits high performance as well as excellent fault tolerance.

It is worth noting that despite physical, thermal and electrical isolation, the different 3-phase sets are not magnetically isolated. Each 3-phase set cannot be regarded as an independent unit in fault conditions. The triple 3-phase machine drive has 6 independent current variables ($i_{d1}, i_{q1}, i_{d2}, i_{q2}, i_{d3}, i_{q3}$). Together with the rotor position, the machine flux linkages are non-linear functions of 7 variables. Direct FE simulations of various fault behaviors are possible [16], but the process would not be effective to identify the worse cases and to provide physical insights of how control parameters and operating conditions influence the fault behaviors. Co-simulation of the machine FE model and the inverter circuit model together with the control law and mechanical system model is prohibitively slow. And it is extremely difficult to assess system behavior and to develop post-fault control law and fault detection techniques over a wide operation region.

In terms of parameter based model [8, 17, 18], it requires the parameters of inductance matrix, PM flux linkages and resistances. However, for the machine under consideration, the inductances are heavily dependent on the rotor angle and the currents of all three sets with 7 independent variables. In addition, because of magnetic saturation, it is extremely difficult to separate the flux linkages from those of rotor PM field. Flux-linkage map based model is also feasible for multi-phase machines [19, 20], however, computationally efficient model capable of predicting multiple 3-phase machine drive under healthy and fault conditions has not been reported in literature. With the conventional flux-linkage map based approach, 7D lookup tables are required, which becomes impossible to construct by FE simulations.

Thus, no existing modelling technique is available to represent this complex machine drive behavior in a computationally efficient manner. To this end, a general modelling technique is proposed for the triple redundant PMA SynRM, accounting for the healthy, open circuit, short circuit and unequal current operation conditions. The machine's MMF distribution is divided into three parts. The machine behavior associated with each 3-phase winding can be described by the rotor position θ , dq frame currents i_d, i_q and an MMF offset component F_{os} . Based on these four variables, the flux linkages and torque of each 3-phase module can be interpolated from 4D tables which effectively reduce the model complexity and accelerate the computation. The proposed model is capable of very fast simulation with the

drive system under various fault and transient conditions, providing great flexibility for assessing the system behavior under different failure modes. It also facilitates the development of the post-fault control and fault detection algorithm. The effectiveness of the model is verified by extensive simulation and experimental tests.

II. GENERAL MACHINE MODELLING

The specifications of the PMA SynRM under study are listed in Table I. The three independent 3-phase windings are denoted as ABC, DEF and GHI, distributed over 360 mechanical degrees. Each 3-phase winding occupies 120 degrees with each phase consisting of two coils in series. By way of example, the turn functions of the coils in set ABC are plotted in Fig. 2 according to the coil displacement [21]. It should be noted that the turn functions of phase C are negative due to the reversed go-return polarity relative to those in phase A and B. The turn functions of set DEF and GHI can be obtained by 120° and 240° phase shift, respectively.

Table I
Specifications and Leading Parameters of the Machine

Specification	Symbol	Value
Base speed	n_b	4000 rpm
Maximum speed	n_m	19 200 rpm
Rated power	P_r	35 kW
Rated current and gamma angle	I_{rated}	120 A(51°)
Nominal DC link voltage	V_{dc}	270 V
Line to line bmf at n_m		246.4 V
Stator radius	R_s	90 mm
Rotor radius	R_r	51.75 mm
Stack length	L	110 mm
Turn number of each coil	N	8

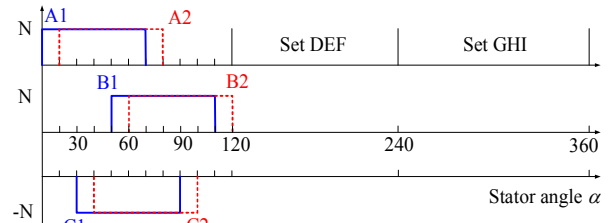


Fig. 2. Turn functions of the coils in set ABC.

Since the airgap is uniform, the winding function of each coil is derived as in (1) where $n_k(\alpha)$ denotes the variation of the turn function of coil k with the angular displacement α in the airgap while $\langle n_k(\alpha) \rangle$ represents the average value of $n_k(\alpha)$ over the whole airgap [22]:

$$N_k(\alpha) = n_k(\alpha) - \langle n_k(\alpha) \rangle \quad (1)$$

In healthy condition, the currents of each 3-phase set are the same, however the currents will differ in case of a fault. Hence, the MMF induced by each set is analyzed and its influence over other sets is investigated. The MMF produced by set ABC can be calculated by multiplying the winding function with relevant currents as in (2) [23].

$$MMF_{ABC}(\alpha) = \sum_{k=A1, A2, \dots, C2} N_k(\alpha) i_k \quad (2)$$

For the sake of discussion, the ampere-turns of each coil with rated current are denoted as 1pu. Assuming at time

instant $t = 0$, the phase currents are $i_A = 1pu$, $i_B = i_C = -0.5pu$, according to equation (2), the MMF produced by set ABC is plotted in Fig. 3.

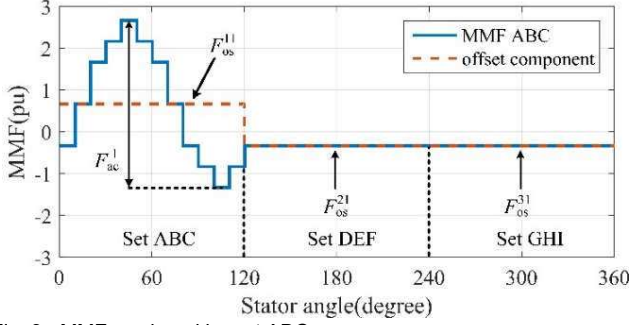


Fig. 3. MMF produced by set ABC.

As can be seen, the currents in set ABC produce MMF not only over the set itself, but also over the other two sets. More specifically, the MMF over set ABC consists of an AC component and an offset component while only an offset component exists over the other sets regions. They can be expressed as:

$$MMF_{ABC} = \begin{cases} F_{ac}^1 + F_{os}^{11} & 0^\circ \leq \alpha < 120^\circ \\ F_{os}^{21} & 120^\circ \leq \alpha < 240^\circ \\ F_{os}^{31} & 240^\circ \leq \alpha < 360^\circ \end{cases}$$

$$F_{ac}^1 = \sum_{n=1,3,5,\dots} A_n \cos(3n\alpha + \delta_n)$$

$$F_{os}^{11} = \frac{2}{3}(i_A + i_B - i_C)$$

$$F_{os}^{21} = -\frac{1}{3}(i_A + i_B - i_C)$$

$$F_{os}^{31} = -\frac{1}{3}(i_A + i_B - i_C)$$
(3)

where F_{ac}^1 is the MMF AC component of the set ABC, A_n and δ_n denote the amplitude and phase angle of the n^{th} MMF harmonic which are functions of the phase currents [24]. The $F_{os}^{i,j}$ represents the MMF offset component over set i caused by set j . Set ABC, DEF and GHI are denoted as sets 1, 2, and 3, respectively.

The analysis above is made on set ABC only. In fact, the MMFs produced by other two sets can be obtained with appropriate phase shifts as shown in Fig. 4. The resultant MMF AC components and offset components can be calculated similarly as in (3).

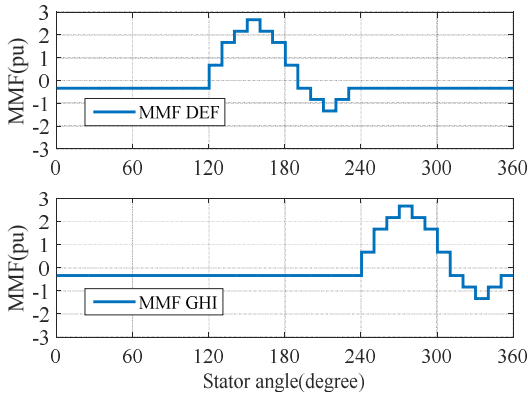


Fig. 4. MMF produced by set DEF and GHI.

It is seen that the currents in each set only produce the AC component only in the region occupied by the set itself while they induce offset component over other sets. In fact, different 3-phase sets affect each other via this offset component. The total MMF over one set region can be obtained by adding the MMF contributions of all three sets. For the simplicity, the total MMF over set ABC, denoted as F^1 , is expressed as:

$$F^1 = F_{ac}^1 + F_{os}^1$$

$$F_{os}^1 = F_{os}^{11} + F_{os}^{12} + F_{os}^{13}$$

$$= \frac{2}{3}(i_A + i_B - i_C) - \frac{1}{3}(i_D + i_E - i_F)$$

$$- \frac{1}{3}(i_G + i_H - i_I)$$
(4)

The total MMF over set ABC is still composed of an AC component and offset component. The AC component is only dependent on the currents in the set itself and rotor position while the offset component is the combined effect of the currents in all three sets but it is independent of rotor position. Due to nonexistence of zero sequence current, the phase currents i_A, i_B, i_C can be represented as i_{d1}, i_{q1} in dq reference frame with respect to the rotor position θ . Together with the offset component F_{os}^1 , the MMF over set ABC can be determined by a function of $(\theta, i_{d1}, i_{q1}, F_{os}^1)$ as:

$$F^1 = F_{ac}^1 + F_{os}^1 = f(\theta, i_{d1}, i_{q1}, F_{os}^1)$$
(5)

The total MMFs over sets DEF and GHI can be similarly expressed as in (6). The variables are defined similarly as above.

$$F^2 = F_{ac}^2 + F_{os}^2 = f(\theta, i_{d2}, i_{q2}, F_{os}^2)$$

$$F^3 = F_{ac}^3 + F_{os}^3 = f(\theta, i_{d3}, i_{q3}, F_{os}^3)$$
(6)

where,

$$F_{os}^2 = \frac{2}{3}(i_D + i_E - i_F) - \frac{1}{3}(i_A + i_B - i_C)$$

$$- \frac{1}{3}(i_G + i_H - i_I)$$

$$F_{os}^3 = \frac{2}{3}(i_G + i_H - i_I) - \frac{1}{3}(i_A + i_B - i_C)$$

$$- \frac{1}{3}(i_D + i_E - i_F)$$
(7)

It can be shown that under healthy conditions the dq currents of each set are the same, the offset components are cancelled according to (4) and (7) and all three sets will produce the same AC component as in a 3-phase machine. In case of one set open circuit condition, the AC component is zero for the fault set due to zero phase currents and the offset component still exists due to the other sets, whilst the other sets exhibit both an AC and offset component. If one set is short circuited, short circuit currents will flow in the fault set. The resultant MMF can be deduced accordingly as a combination of the AC component and offset component for each set. In the extreme condition where the currents in each set are all different, the MMF of each set can still be expressed by (5) and (6).

Therefore, it follows that in any conditions the MMF over the whole airgap can be divided into three parts. Each of them is associated with a 3-phase set and can be expressed by $f(\theta, i_d, i_q, F_{os})$ where i_d, i_q are the currents in that set while F_{os} is the combined offset component due to all three sets.

With the help of MMF decomposition, the influence of other two sets currents is represented as single variable, the offset component F_{os} , therefore reducing system complexity effectively.

The flux density in the airgap depends on the MMF and PM field whose combined effect determines the flux linkages and torque. Therefore that flux linkages and torque of one 3-phase set are determined by the MMF over that set expressed by $f(\theta, i_d, i_q, F_{os})$. In other words, the flux linkages and torque of one 3-phase set are functions of the four variables $(\theta, i_d, i_q, F_{os})$. The relationships can be stored in 4D lookup tables which can be established by FE analysis as will be described in section III. As a result, the behavior of each 3-phase set can be predicted by interpolating the 4D tables via the 4 variables $(\theta, i_d, i_q, F_{os})$.

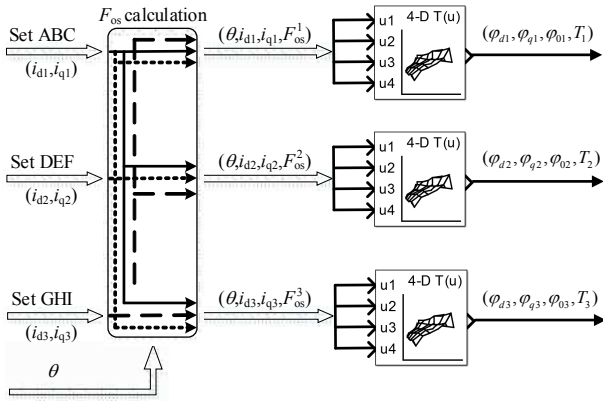


Fig. 5. General modelling diagram.

Thus, a general modelling method is proposed as shown in Fig. 5. The currents of all three 3-phase set together with rotor angle θ are fed into the MMF offset calculation block to deduce F_{os} for each set according to (4) and (7). Then the 4 variables $(\theta, i_{di}, i_{qi}, F_{os}^i, i = 1, 2, 3)$ which describe the MMF of each set are obtained. These 4 variables form the inputs to the 4D tables and the resultant $dq\theta$ axis flux linkages $(\varphi_{di}, \varphi_{qi}, \varphi_{oi})$ and torque of that 3-phase set T_i can be obtained. It should be noted that the flux linkages and torque of each set are interpolated separately. The total torque is obtained by adding the torque contribution of all three sets. The voltage equations of each 3-phase set are expressed as:

$$\begin{aligned} u_{di} &= Ri_{di} + \frac{d\psi_{di}}{dt} - \omega\psi_{qi} \\ u_{qi} &= Ri_{qi} + \frac{d\psi_{qi}}{dt} + \omega\psi_{di} \end{aligned} \quad (8)$$

The u_{di}, u_{qi} denote the applied voltages in dq axis while R represents the phase resistance. As can be seen, the influence of other two sets currents has been simplified by F_{os}^i , and hence the dimension of lookup table is reduced. Thus the machine behavior can be fully captured by interpolating the 4D tables with the voltage equations for each set. The proposed modelling method is capable to predict the machine behavior under healthy, open circuit, short circuit and unequal currents operating conditions, etc. without any modification, which save significant efforts to predict the machine

performance under different conditions.

III. 4D TABLE CONSTRUCTION

As discussed above, the flux linkages and torque of one 3-phase set are dependent on the MMF over that set and hence they are functions of the four variables $(\theta, i_d, i_q, F_{os})$. Thus, the remaining task is to construct the flux linkages and torque lookup tables of one 3-phase set which are resultant from the MMF. Since the machine under consideration is subject to magnetic saturation, FE analysis is performed to extract the data for the 4D tables. It is worth noting that the three 3-phase sets are identical because the electrical phase shift between each set is 360° . The same MMF will lead to the same behavior for the three 3-phase sets. Therefore, the 4D tables only need to be constructed for one 3-phase set and the other two sets can use the same tables. Hence, FE simulations are performed to extract the flux linkage and torque data of set ABC based on the full machine model.

The key of table construction is to generate the MMF over set ABC defined by $f(\theta, i_d, i_q, F_{os})$. As discussed previously, the MMF AC component is purely determined by the currents of its own set. Thus, for given (θ, i_d, i_q) , the phase currents of set ABC can be derived by dq transform as:

$$\begin{aligned} i_A &= i_d \cos 3\theta - i_q \sin 3\theta \\ i_B &= i_d \cos(3\theta - 120^\circ) - i_q \sin(3\theta - 120^\circ) \\ i_C &= i_d \cos(3\theta + 120^\circ) - i_q \sin(3\theta + 120^\circ) \end{aligned} \quad (9)$$

However, the MMF offset component F_{os} is combined effect of the currents in all three 3-phase sets. To represent this offset component, specific currents should be injected to sets DEF and GHI to generate the required F_{os} . Hence, the currents in sets DEF and GHI are specified as (10) where x, y, z are appropriate values to be determined to produce the required F_{os} :

$$\begin{aligned} i_D &= i_G = i_A + x \\ i_E &= i_H = i_B + y \\ i_F &= i_I = i_C + z \end{aligned} \quad (10)$$

The resultant F_{os} over set ABC is derived by substituting (9) and (10) into (4) as:

$$F_{os} = -\frac{2}{3}(x + y - z) \quad (11)$$

Zero sequence current cannot circulate, therefore:

$$x + y + z = 0 \quad (12)$$

Based on (11) and (12), it can be deduced that:

$$\begin{aligned} x + y &= -\frac{3}{4}F_{os} \\ z &= \frac{3}{4}F_{os} \end{aligned} \quad (13)$$

In order to obtain a unique solution for x, y , their values should be chosen as to minimize the saturation effect. Thus, x, y are defined as:

$$x = y = -\frac{3}{8}F_{os} \quad (14)$$

which results in the lowest peak value over one electrical period for phases D, E and G, H . Therefore, for a given set of $(\theta, i_d, i_q, F_{os})$, their physical effect is replicated over set ABC by injecting the currents in (9) and (10) in the machine 2D FE model, and the resultant flux linkage and torque are

calculated for the region of ABC set. The flux linkages are directly obtained from flux sensors whilst the torque is calculated by Maxwell stress tensor in the airgap under set ABC. The Maxwell stress tensor integration is performed based on a closed circle the airgap. And the integration over set ABC region is taken as the torque contribution due to the MMF defined by $f(\theta, i_d, i_q, F_{os})$. It is worth noting that the high nonlinearity effects, like slot effect, space harmonics and cross saturation, are considered by the FE model directly.

The 4D lookup table data are extracted by varying i_d over $[-100A, 0A]$, i_q over $[0A, 100A]$ in steps of 20A and F_{os} over $[-160, 160]$ in steps of 40 over one electrical cycle with variation of rotor position from 0 to 120°(mech.) in steps of 2.5° in FE simulations. It took 10 days to complete the FE computation on a desktop PC which is main shortcoming of the model approach. However, once the tables are obtained, the model can be simulated within 10 seconds using linear interpolation for most drive operations. The model can be readily integrated with inverter, control law and mechanical load, facilitating the fault behavior assessment, post fault control and detection development. The accuracy of the proposed model will be examined by FE simulation and experimental tests.

IV. SIMULATION VALIDATION

In this section, the accuracy of the proposed modelling method is examined by comparing the prediction with FE results under healthy, open circuit, short circuit and unequal current conditions. The currents of the three sets ($i_{d1}, i_{q1}, i_{d2}, i_{q2}, i_{d3}, i_{q3}$) are directly defined in the FE for a given operating condition, and the machine behavior is computed. The same operating conditions are simulated with the proposed model shown in Fig. 5. The same currents commands are used to calculate the MMF offset F_{os} for each 3-phase according to (4) and (7), the results are fed into the 4D lookup tables to obtain the flux linkages and torques.

A. Healthy Operation

Under healthy condition, the currents in each set are the same. Thus, the F_{os} is zero for all the three 3-phase sets. The machine behavior is purely determined by (θ, i_d, i_q) . It becomes similar with the high fidelity modelling technique discussed in [19]. For the purpose of validation in a wide load range, tests is conducted at the based speed with the rated and half rated currents. The gamma angle, which is the current vector angle with respect to the q -axis, for both cases is set as 51°. The predicted results together with the FE results are compared in Fig. 6 and Fig. 7. They show that the model and FE predicted flux linkages and torques are essentially the same for the two cases.

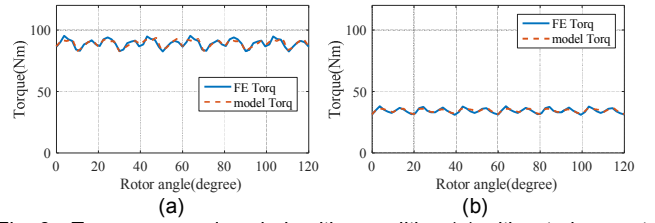


Fig. 6. Torque comparison in healthy condition (a) with rated current excitation (b) with half rated current excitation.

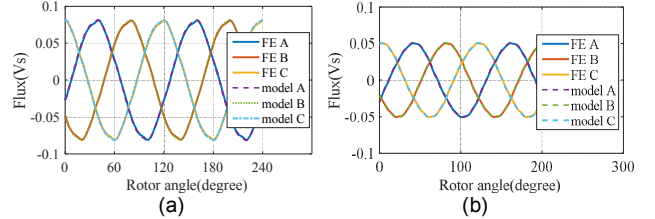


Fig. 7. Comparison of flux linkages in set ABC in healthy condition (a) with rated current excitation (b) with half rated current excitation.

B. Open Circuit

An open circuit fault is assumed in set ABC, the phase currents are set as zero. Whilst sets DEF and GHI are still excited with the rated currents and half rated as the healthy condition respectively. Thus, the currents of set ABC are zero while other sets' currents remain unchanged.

Fig. 8 and Fig. 9 compare the torques and flux linkages predicted by the model and FE for the both test cases. As can be seen, the model-predicted torque follows the main trend of the FE result, albeit being slightly higher. 2nd harmonic is observed in the waveform which is captured by the prediction. The 2nd harmonic torque ripple increases with the load currents due to the increased asymmetry between different sets. It is caused by the higher MMF offset component which indicates the mutual coupling between different sets. Since the behaviors of sets DEF and GHI are similar, only the results of set DEF are compared. The predicted flux linkages also match well with the FE results with small errors for both cases. It is noticed that the flux linkages are no longer balanced under the fault condition which confirms mutual coupling between three sets through the MMF offset component.

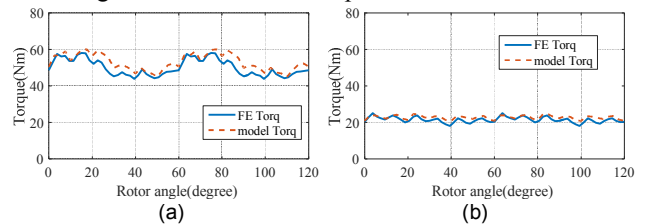


Fig. 8. Torque comparison in open circuit condition (a) with rated current excitation (b) with half rated current excitation.

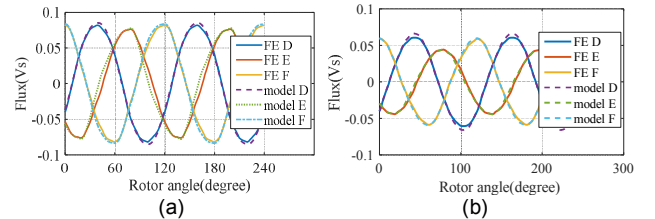


Fig. 9. Comparison of flux linkages in healthy set (a) with rated current excitation (b) with half rated current excitation.

C. Short Circuit

In case of a switch or winding short circuit, terminal short circuit is applied to the fault set to mitigate the fault. Hence, u_{d1} and u_{q1} are set as zero in FE and the model for set ABC where the fault occurs. The induced short circuit currents are determined by the flux linkages of the faulty set. Since the 3-phase winding is star connected, zero sequence current is 0. Thus, the short circuit currents are governed by (15), and F_{os} of each 3-phase set can be calculated similarly by (4) and (7).

$$\begin{aligned} i_{d1} &= (\omega\psi_{q1} - \frac{d\psi_{d1}}{dt})/R \\ i_{q1} &= -(\omega\psi_{d1} + \frac{d\psi_{q1}}{dt})/R \end{aligned} \quad (15)$$

The behavior of the machine is evaluated with set ABC terminal short circuited while the other sets are excited with the rated and half rated currents respectively. The currents in set ABC is obtained from (15) with the dq flux linkages predicted by the model. The model predicted torques match well with the FE results as shown in Fig. 10. Good agreements are also observed in the short-circuit currents and the flux linkages comparisons in Fig. 11-Fig. 13. It is seen that the short-circuit currents in each phase of the ABC set are asymmetrical. The flux linkages in the faulty set are effectively nullified except for the zero sequence components due to the MMF offset. The two test cases, under rated and half rated currents excitations, confirm that the model has high accuracy in most operation range.

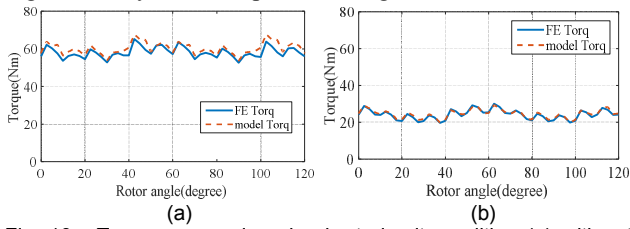


Fig. 10. Torque comparison in short circuit condition (a) with rated current excitation (b) with half rated current excitation.

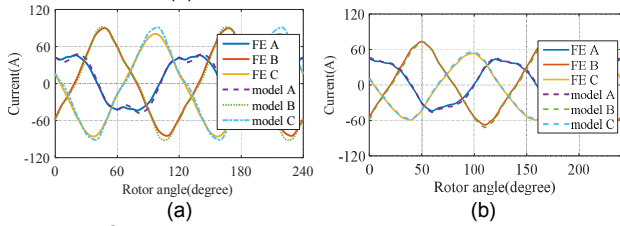


Fig. 11. Short circuit currents comparison (a) with rated current excitation (b) with half rated current excitation.

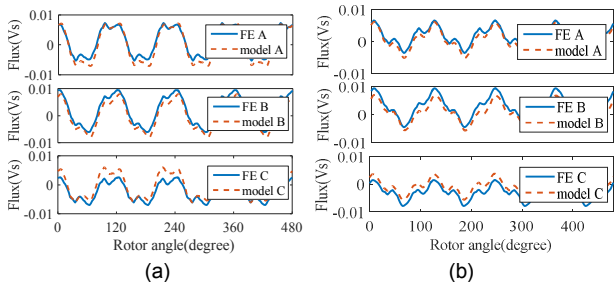


Fig. 12. Comparison of flux linkages in the short circuit set (a) with rated current excitation (b) with half rated current excitation.

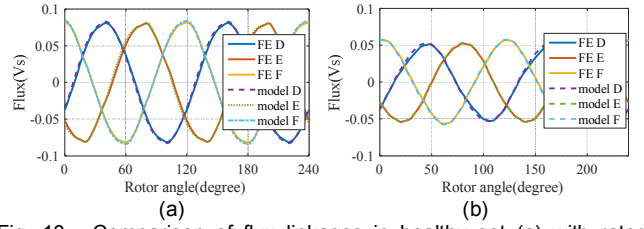


Fig. 13. Comparison of flux linkages in healthy set (a) with rated current excitation (b) with half rated current excitation.

D. Unequal Current Operation

In practical applications, the currents in each set may be unequal due to limited current control bandwidth and current sensor accuracy, leading to unequal current operation mode in the three 3-phase sets. Without loss of generality, the unequal current operation is exaggerated by assuming that set ABC has 1pu current excitation, while set DEF and GHI have 0.9pu and 0.8pu current, respectively. The gamma angle is set as 51° for all three sets. The predicted flux linkages and torque are compared with the FE results in Fig. 14 and Fig. 15. Since the flux linkages of three sets are similar, only the flux linkages of set ABC are compared.

The two predicted results coincide with each other. In addition, with the proposed model, the torque contribution of each set can be identified as in Fig. 15 providing more insight into the machine behavior. The torque contribution of each set increases with the current. Set ABC is excited with the highest current, therefore inducing the maximum MMF AC component which is the working harmonic. It reacts with the PM field and rotor saliency and hence produces the highest torque among the three 3-phase sets.

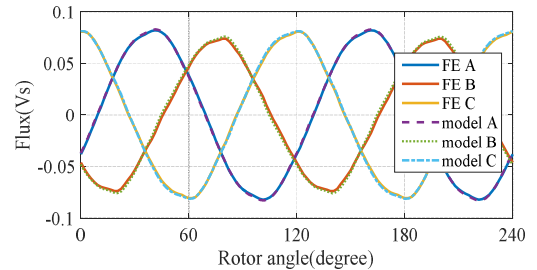


Fig. 14. Flux linkages comparison of set ABC.

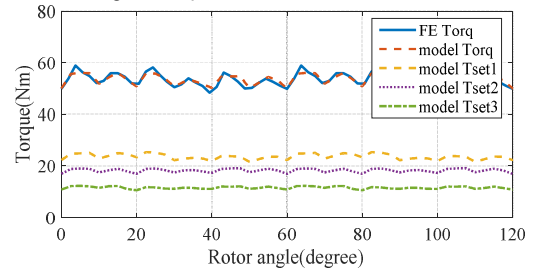


Fig. 15. Torque comparison in unequal current operation.

V. EXPERIMENTAL VALIDATION

The proposed modelling technique has been tested on a 9 phase PMA SynRM drive whose specifications are given in Table I. The machine prototype is shown in Fig. 16. The windings of different 3-phase sets are effectively separated by the segregated windings. The machine is mounted on the

dynamometer via the torque transducer as in Fig. 17. The dynamometer operates at a given speed while the machine under tests is driven by a DSP based 9 phase inverter, consisting of three standard 3-phase inverters as in Fig. 18. The machine behavior is the same as the conventional 3-phase configuration and the behavior of the three sets are the same. So the conventional vector control is employed to control the machine drive. The three inverter drive modules share the same current references from the speed controller but track them by independent current controllers. Hence, failure in one 3-phase set does not significantly affect the operation of the other sets. And each drive could response properly in case of a fault. The machine drive is tested under healthy operation, one set open circuit, short circuit, unequal current and transient modes. The measured currents, voltages and torque are compared with model predicted results. All the tests are performed at the base speed of 4000rpm unless otherwise stated.

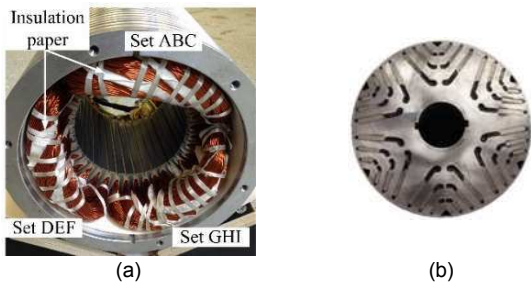


Fig. 16. The 9 phase PMA SynRM prototype (a) stator with segregated windings (b) rotor stack.

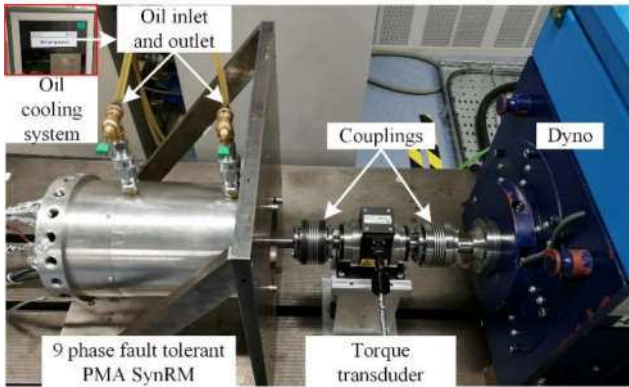


Fig. 17. The 9 phase PMA SynRM test rig.



Fig. 18. DSP based 9 phase inverter.

A. Healthy Condition

First the machine is tested in healthy mode with each set fed with 80A currents under the maximum torque per Ampere (MTPA) operating condition. The test results are compared with the model prediction in Fig. 19 and Fig. 20. The

measured currents match well with the predicted results. The machine is fed by inverter switching at 10kHz. Due to the limited current probes of the oscilloscope, the 9 phase currents are mainly measured by the inverter current sensors and stored in the DSP RAM, and consequently the switching harmonics are not visible due to limited sampling frequency and anti-alias filtering. The predicted voltages are quite close to the test results, though, with small error and less harmonics. It should be noted that the test dq voltages are the control reference voltages in the DSP. Therefore, they are slightly different from the real voltages applied to the motor.

As shown in the top of Fig. 21, the torque predictions are compared with measurements in healthy condition varying the current from 0 to 120A in MTPA condition. Due to the limited bandwidth of the torque transducer, the torque ripple cannot be captured and only the mean torque is compared. It is shown that the measured torque is a few percent lower than prediction. According to previous simulation validation, the flux linkages and torque predictions match well with FE calculations. Thus the torque error is mainly caused by the inaccuracy of the 2D FE model as well as neglecting the frictional and windage torque in the model. Since the lookup tables are generated based on the FE model, similar error would be expected in other operation conditions.

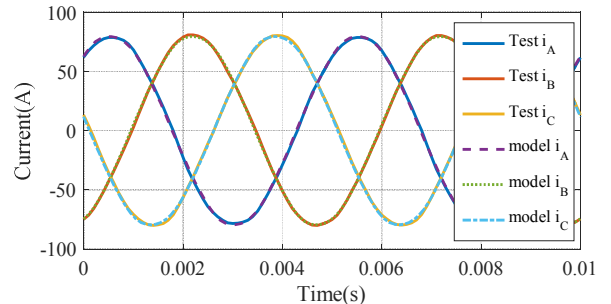


Fig. 19. Comparison of measured and predicted currents in healthy mode.

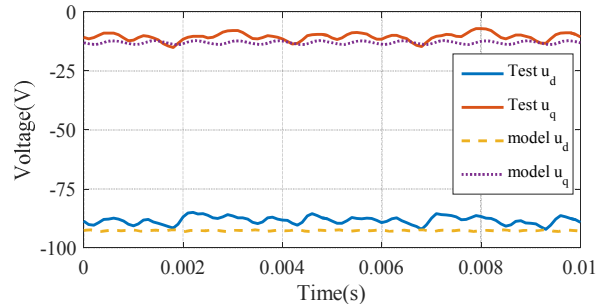


Fig. 20. Comparison of measured and predicted voltages in healthy mode.

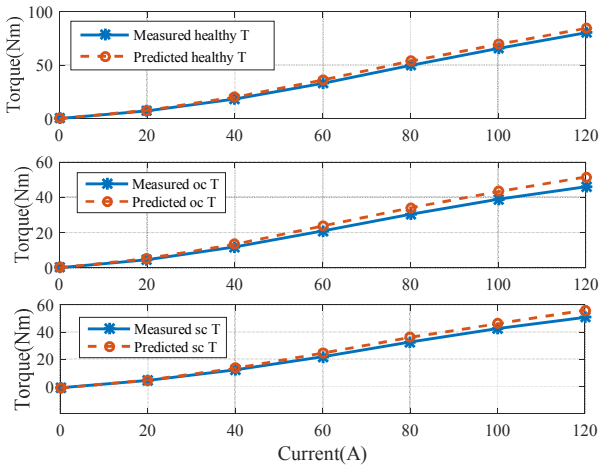


Fig. 21. Comparison of measured and predicted torques in healthy, open circuit, short circuit conditions.

B. One Set Open Circuit

The machine drive is tested with one set open circuit when set ABC is open circuited by switching off all the respective IGBTs. Set DEF and GHI are still excited with 80A currents. The measured results for set DEF are compared with the predictions in Fig. 22 and Fig. 23. Similar behaviors of set GHI are observed but are not shown. In the open circuit mode, the phase currents in DEF set are no longer balanced with noticeable distortion due to insufficient control bandwidth. These unbalance and distortions are well captured by the model with small deviation from the measured current waveforms. The control voltages are also close to the predictions in which the induced 2nd harmonics in the dq voltages are captured.

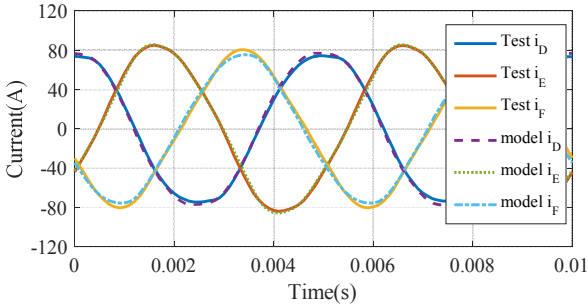


Fig. 22. Comparison of measured and predicted currents in open circuit mode.

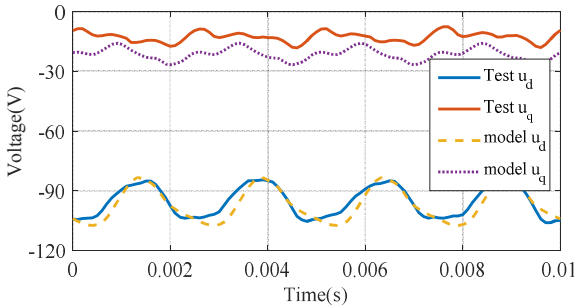


Fig. 23. Comparison of measured and predicted voltages in open circuit mode.

Though set ABC is open circuited, the currents in other two healthy sets still generates torque for continued operation.

The measured torque is compared with the model prediction in the middle of Fig. 21 with a few percent lower. The difference may be caused by errors in the FE model and current prediction. As can be seen, the machine drive is capable to provide about 2/3 of the healthy torque in open circuit condition. Thus, the open circuit fault can be coped with.

Due to the odd number of pole pairs, unbalanced radial force appears with one set open circuited. Increased noise and vibration have been noticed during experimental tests but they are below the maximum permissible level. Post fault operation is not affected and the currents are well controlled. In order to eliminate the unbalanced radial force, the machine can be configured as 6 pole pairs with the two diagonal 3-phase windings connected in series or parallel as one 3-phase set as in [25].

C. One Set Short Circuit

The machine is also tested with one set short circuit. Set ABC is short circuited by setting the d - and q -axis voltage commands to zero in the controller while set DEF and GHI are still excited with healthy currents as previously stated. First, the measured and predicted short circuit currents in set ABC are plotted in Fig. 24. It is seen that the peak short circuit current value is no more than 80A causing no thermal risk to the machine. This can attributed to the low PM field of the PMA SynRM machine. The model has captured the main shapes of the unequal phase currents, being slightly higher than the measurements. The error could be attributed to the additional impedance of the cable leads and the voltage drops on the switches. Again, the measured currents and voltages of the healthy sets are very close to the predictions in Fig. 25 and Fig. 26.

The short circuit currents set ABC do not contribute to the torque whilst the currents in other two sets still generates torque. The measured torque is compared with the model prediction in the bottom of Fig. 21 with different load currents. The a few percents difference is also caused by the error in the FE model and the current prediction. As can be seen, the machine drive is also capable to provide about 2/3 of the healthy torque/power in short circuit condition. Thus, the short circuit fault can be accommodated.

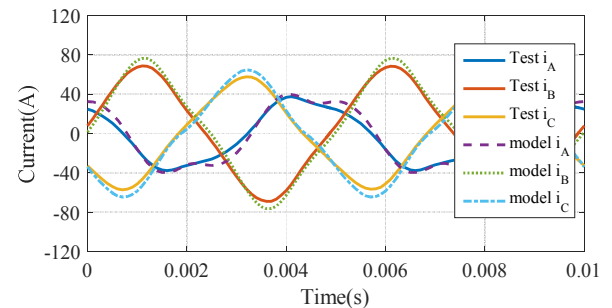


Fig. 24. Comparison of measured and predicted short circuit currents.

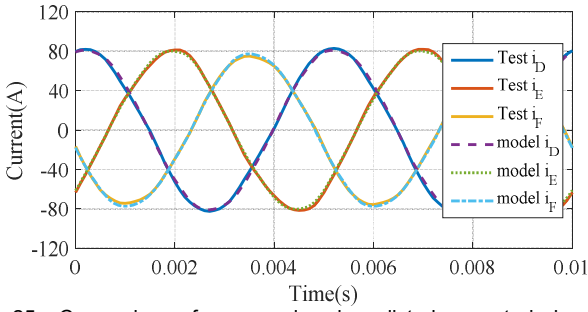


Fig. 25. Comparison of measured and predicted currents in healthy DEF set when set ABC in short circuit mode.

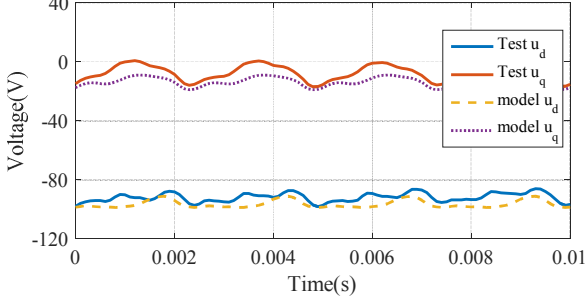


Fig. 26. Comparison of measured and predicted voltages in healthy DEF set when set ABC in short circuit mode.

D. Unequal Current Operation

Then the machine drive is tested under unequal current operation. Set ABC is fed with 100A, while set DEF and GHI are fed with 80A and 60A, respectively. The measured and predicted currents and voltages of set ABC are compared in Fig. 27 and Fig. 28 while the results of other two sets are similar and omitted. The results show that the behavior under this mode is also well represented by the model albeit mismatches in high order harmonics exist.

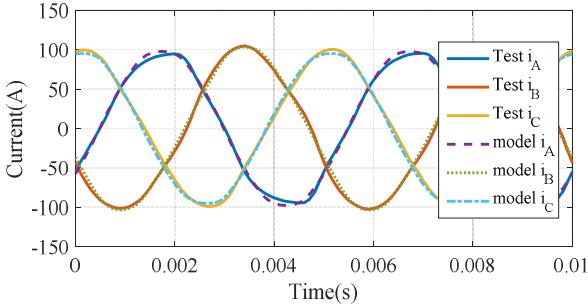


Fig. 27. Comparison of measured and predicted phase currents in set ABC under unequal currents operation.

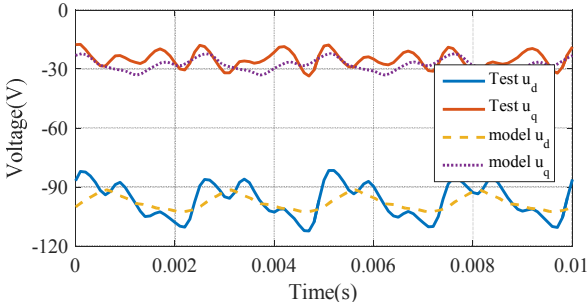


Fig. 28. Comparison of measured and predicted voltages in set ABC under unequal currents operation.

E. Transient Process

Finally, an integrated fault and mitigation test is performed at 2000rpm to represent the machine transient behavior. Initially, the machine is operating in healthy condition with 60A excitation as shown in Fig. 29. Then a fault is injected at 0.013s in set ABC where the disturbance can be seen. The fault is quickly detected and the mitigation action, terminal short circuit is applied on the ABC set at 0.017s. As can be seen, the currents in set ABC oscillate due to the application of terminal short circuit and they decay gradually. The measured and predicted currents in the transient agree reasonably well. In addition, the currents in set DEF are also well predicted as shown in Fig. 30. The impact of terminal short circuit on set DEF currents is insignificant due to good isolation between the sets. Thus, the model is capable to predict the machine behavior in transient condition.

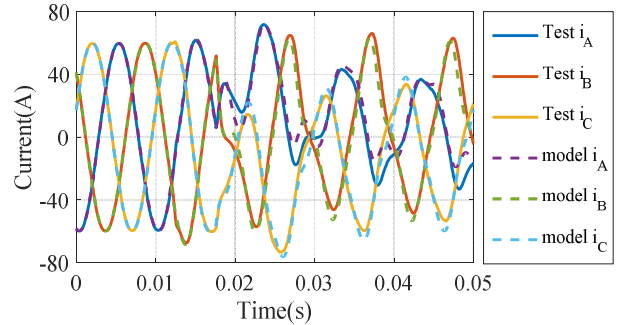


Fig. 29. Comparison of measured and predicted currents of set ABC in transient process.

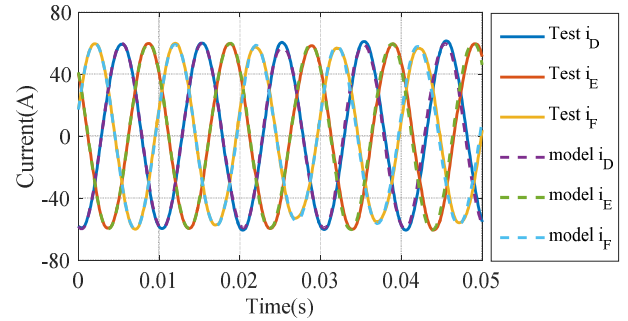


Fig. 30. Comparison of measured and predicted currents of set DEF in transient process.

VI. CONCLUSION

In this paper, a general modelling technique has been proposed for a triple redundant, fault tolerant 3x3-phase PMA SynRM capable of accurately predicting the behavior in all operating modes, including the healthy operation, open circuit, short circuit, unequal current operation and even transient process. The accuracy of the modelling technique has been validated by extensive FE simulations and experimental tests. The proposed modelling technique can be extended to other multiple 3-phase machines with similar winding configuration, providing a useful aid for the performance verification under normal and abnormal conditions as well as for the design and development of fault detection and fault-tolerant control strategies.

VII. REFERENCES

- [1] V. I. Patel, J. Wang, D. T. Nugraha, R. Vuletic, and J. Tousen, "Enhanced Availability of Drivetrain Through Novel Multiphase Permanent-Magnet Machine Drive," *Industrial Electronics, IEEE Transactions on*, vol. 63, pp. 469-480, 2016.
- [2] W. Cao, B. C. Mecrow, G. J. Atkinson, J. W. Bennett, and D. J. Atkinson, "Overview of Electric Motor Technologies Used for More Electric Aircraft (MEA)," *Industrial Electronics, IEEE Transactions on*, vol. 59, pp. 3523-3531, 2012.
- [3] W. Wang, M. Cheng, B. Zhang, Y. Zhu, and S. Ding, "A Fault-Tolerant Permanent-Magnet Traction Module for Subway Applications," *IEEE Transactions on Power Electronics*, vol. 29, pp. 1646-1658, 2014.
- [4] N. Bianchi, S. Bolognani, and M. Zigliotto, "Analysis of PM synchronous motor drive failures during flux weakening operation," in *Power Electronics Specialists Conference, 1996. PESC '96 Record., 27th Annual IEEE*, 1996, pp. 1542-1548 vol.2.
- [5] N. Bianchi and S. Bolognani, "Design of a Fault-tolerant IPM Motor for Electric Power Steering," in *Power Electronics Specialists Conference, 2005. PESC '05. IEEE 36th*, 2005, p. 2873.
- [6] D. C. Patel and M. C. Chandorkar, "Modeling and Analysis of Stator Interturn Fault Location Effects on Induction Machines," *IEEE Transactions on Industrial Electronics*, vol. 61, pp. 4552-4564, 2014.
- [7] B. Sen and J. Wang, "Analytical modelling of stator turn fault in surface mounted permanent magnet machines," in *Energy Conversion Congress and Exposition (ECCE), 2013 IEEE*, 2013, pp. 4445-4452.
- [8] O. A. Mohammed, Z. Liu, S. Liu, and N. Y. Abed, "Internal Short Circuit Fault Diagnosis for PM Machines Using FE-Based Phase Variable Model and Wavelets Analysis," *Magnetics, IEEE Transactions on*, vol. 43, pp. 1729-1732, 2007.
- [9] L. Romeral, J. C. Urresty, J. R. Riba Ruiz, and A. Garcia Espinosa, "Modeling of Surface-Mounted Permanent Magnet Synchronous Motors With Stator Winding Interturn Faults," *Industrial Electronics, IEEE Transactions on*, vol. 58, pp. 1576-1585, 2011.
- [10] A. Pantea, A. Yazidi, F. Betin, M. Taherzadeh, S. Carriere, H. Henao, et al., "Six-Phase Induction Machine Model for Electrical Fault Simulation Using the Circuit-Oriented Method," *IEEE Transactions on Industrial Electronics*, vol. 63, pp. 494-503, 2016.
- [11] R. Hyung-Min, K. Ji-Woong, and S. Seung-Ki, "Synchronous-frame current control of multiphase synchronous motor under asymmetric fault condition due to open phases," *IEEE Transactions on Industry Applications*, vol. 42, pp. 1062-1070, 2006.
- [12] X. Tu, L. A. Dessaint, M. E. Kahel, and A. O. Barry, "A New Model of Synchronous Machine Internal Faults Based on Winding Distribution," *IEEE Transactions on Industrial Electronics*, vol. 53, pp. 1818-1828, 2006.
- [13] K. Kyung-Tae, P. Jun-Kyu, H. Jin, and K. Byeong-Woo, "Comparison of the Fault Characteristics of IPM-Type and SPM-Type BLDC Motors Under Inter-Turn Fault Conditions Using Winding Function Theory," *Industry Applications, IEEE Transactions on*, vol. 50, pp. 986-994, 2014.
- [14] Z. Weidong, B. Fahimi, and S. Pekarek, "A field reconstruction method for optimal excitation of permanent magnet synchronous machines," *IEEE Transactions on Energy Conversion*, vol. 21, pp. 305-313, 2006.
- [15] B. Wang, J. Wang, and A. Griffo, "A Fault Tolerant Machine Drive Based on Permanent Magnet Assisted Synchronous Reluctance Machine" in *Energy Conversion Congress and Exposition (ECCE), 2016 IEEE*, Milwaukee, WI, 2016, pp. 1-8.
- [16] M. Dai, A. Keyhani, and T. Sebastian, "Fault analysis of a PM brushless DC Motor using finite element method," *Energy Conversion, IEEE Transactions on*, vol. 20, pp. 1-6, 2005.
- [17] S. Nandi, "A detailed model of induction machines with saturation extendable for fault analysis," *IEEE Transactions on Industry Applications*, vol. 40, pp. 1302-1309, 2004.
- [18] B. Vaseghi, B. Nahid-mobarakh, N. Takorabet, and F. Meibody-Tabar, "Inductance Identification and Study of PM Motor With Winding Turn Short Circuit Fault," *Magnetics, IEEE Transactions on*, vol. 47, pp. 978-981, 2011.
- [19] X. Chen, J. Wang, B. Sen, P. Lazari, and T. Sun, "A High-Fidelity and Computationally Efficient Model for Interior Permanent-Magnet Machines Considering the Magnetic Saturation, Spatial Harmonics, and Iron Loss Effect," *IEEE Transactions on Industrial Electronics*, vol. 62, pp. 4044-4055, 2015.
- [20] B. Sen, J. Wang, and P. Lazari, "A High-Fidelity Computationally Efficient Transient Model of Interior Permanent-Magnet Machine With Stator Turn Fault," *IEEE Transactions on Industrial Electronics*, vol. 63, pp. 773-783, 2016.
- [21] B. Sen, J. Wang, and P. Lazari, "A detailed transient model of Interior Permanent Magnet motor accounting for saturation under stator turn fault," in *Energy Conversion Congress and Exposition (ECCE), 2013 IEEE*, 2013, pp. 3548-3555.
- [22] N. A. Al-Nuaim and H. Toliyat, "A novel method for modeling dynamic air-gap eccentricity in synchronous machines based on modified winding function theory," *IEEE Transactions on Energy Conversion*, vol. 13, pp. 156-162, 1998.
- [23] J. Faiz, I. T. Ardekani, and H. A. Toliyat, "An evaluation of inductances of a squirrel-cage induction motor under mixed eccentric conditions," *IEEE Transactions on Energy Conversion*, vol. 18, pp. 252-258, 2003.
- [24] X. Chen, J. Wang, V. I. Patel, and P. Lazari, "A Nine-Phase 18-Slot 14-Pole Interior Permanent Magnet Machine With Low Space Harmonics for Electric Vehicle Applications," *IEEE Transactions on Energy Conversion*, vol. 31, pp. 860-871, 2016.
- [25] L. Alberti and N. Bianchi, "Experimental Tests of Dual Three-Phase Induction Motor Under Faulty Operating Condition," *Industrial Electronics, IEEE Transactions on*, vol. 59, pp. 2041-2048, 2012.



Bo Wang (M'17) received the B.Eng. and M.Sc. degrees in electrical engineering from Nanjing University of Aeronautics and Astronautics, Nanjing, China, in 2009 and 2012, respectively. Since 2014, he has been working toward the Ph.D. degree at the Department of Electronic and Electrical Engineering, University of Sheffield, Sheffield, U.K.

From 2012 to 2014, he served as a senior engineer in the Delta Electronics Co. Ltd. Currently, he is working as a research associate at the Department of Electronic and Electrical Engineering, University of Sheffield. His research interests include the permanent magnet machine drives, electric traction and fault tolerant systems.



Jibin Wang (SM'03) received the B.Eng. and M.Eng. degrees from Jiangsu University, Zhenjiang, China, in 1982 and 1986, respectively, and the Ph.D. degree from the University of East London, London, U.K., in 1996, all in electrical and electronic engineering.

Currently, he is a Professor in Electrical Engineering at the University of Sheffield, Sheffield, U.K. From 1986 to 1991, he was with the Department of Electrical Engineering at Jiangsu University, where he was appointed a Lecturer in 1987 and an Associated Professor in 1990. He was a Postdoctoral Research Associate at the University of Sheffield, Sheffield, U.K., from 1996 to 1997, and a Senior Lecturer at the University of East London from 1998 to 2001. His research interests range from motion control and electromechanical energy conversion to electric drives for applications in automotive, renewable energy, household appliances and aerospace sectors.

He is a fellow of the IET and a senior member of IEEE.



Antonio Griffo (M'13) received the M.Sc. degree in electronic engineering and the Ph.D. degree in electrical engineering from the University of Napoli "Federico II," Naples, Italy, in 2003 and 2007, respectively. From 2007 to 2013, he was a Research Associate with the University of Sheffield, Sheffield, U.K., and the University of Bristol, Bristol, U.K. He is currently a Lecturer with the Department of Electronic and Electrical Engineering, University of Sheffield. His research interests include modeling, control and condition monitoring of electric power systems, power electronics converters, and electrical motor drives, for renewable energy, automotive and aerospace applications.



Bhaskar Sen (M'17) received the B.E. degree from the Delhi College of Engineering, Delhi, India, in 2003, the M.Tech. degree from the Indian Institute of Technology, Kanpur, India, in 2006, both in electrical engineering, and the Ph.D. degree in electrical and electronic engineering from The University of Sheffield, Sheffield, U.K., in 2015. From 2006 to 2011, he was a Research Engineer with GE Global Research, Bangalore, India. From 2015 to 2017, he was a Research Associate at The University of Sheffield. His research interests include electrical machine fault modeling, machine fault detection, and fault-tolerant drives.